**RESEARCH ARTICLE**

# Analysis of the microstructural connectivity and compressive behavior of particle aggregated silica aerogels

**Weibo Xiong**[1] ◉ | **Rasul Abdusalamov**[1] ◉ | **Mikhail Itskov**[1] | **Barbara Milow**[2] | **Ameya Rege**[2] ◉

[1]Department of Continuum Mechanics, RWTH Aachen University, Aachen, Germany

[2]Department of Aerogels and Aerogel Composites, Institute of Materials Research, German Aerospace Center, Cologne, Germany

**Correspondence**
Weibo Xiong, Department of Continuum Mechanics, RWTH Aachen University, Eilfschornsteinstr. 18, 52062 Aachen, Germany.
Email: xiong@km.rwth-aachen.de

**Abstract**

Porous media such as aerogels can exhibit unique properties including low thermal conductivity, low bulk density, and low sound velocity. However, the limited mechanical properties of aerogels restrict their widespread application. This study focuses on understanding the mechanical behavior of aggregated silica aerogels by investigating their microstructural connectivity and densification mechanisms under uniaxial compression. The interparticle connectivity is generated using the diffusion-limited cluster–cluster aggregation (DLCA) algorithm, and the particle connections are modeled by beam elements that account for contact interaction. The mechanical response of representative volume elements (RVEs) is analyzed in both linear and nonlinear regimes while applying periodic boundary conditions. The model is correlated with experimental compression test data to validate the simulation results. With increasing compressive strain, load transitions between multiple backbone paths appear in the network structure. Thus, the simulation model provides insight into the compression process. Moreover, the simulation model enables the examination of the influence of various model parameters and facilitates the evaluation of the power–law relationship between the elasticity modulus and porosity of aerogels.

## 1 | INTRODUCTION

Aerogels encompass a unique class of materials that originated with Kistler's invention in 1931 using a supercritical drying technique and have persistently drawn the scientific community's attention due to their broad-spectrum application potential [1]. The intrinsic microstructure of aerogels is similar to a three-dimensional, open network of nanoparticles, and is often described as a "pearl necklace" configuration [2]. This unique microstructure gives aerogels exceptional properties such as a large specific surface area (>1000 m$^2$/ g), low thermal conductivity(<0.02 W/mk), and remarkably low density (<0.05 g/cm$^3$) [3, 4]. However, this porous nature also leads to brittleness and limits their wider use beyond pure insulation applications. Understanding the unique mechanical structure–property relationship of silica aerogels is essential to unlock their full potential through reverse engineering.

In the last decade, silica aerogels have been studied computationally in order to gain a deeper understanding of their properties. Two major approaches include molecular dynamics simulations as well as mesoscopic models [1]. With increasing computational power, the length scale differences between these approaches have become less distinct; for instance, Gonçalves et al. have fully atomistically modeled silica aerogels within a 100-nm cube [5]. Although this mesoscale atomistic model is able to capture the structural and mechanical properties, the atomistic nature does not allow for modeling of the sol–gel process, which involves condensation reactions. Currently, the following approaches for sol–gel representation are gaining more attention [1, 6]: (i) algorithm based on the Smoluchowski equation [7, 8], (ii) Langevin dynamics [9, 10], (iii) percolation theory and cluster aggregation models [11–13]. Among these, percolation theory and cluster aggregation have provided significant insights into the internal gel structure [6, 8], correlating synthesis parameters with microstructure [13].

Through computational modeling and experimental investigations [14], the fractal nature of silica aerogels is a well-recognized attribute. These fractal structures, that is, self-similar features discernible at different length scales, are also a prerequisite for coarse-grained models [1]. Using diffusion-limited aggregation approaches, the generated fully gelled network has been shown to be fractal [15]. The generated network is commonly assumed to be the microstructure of aerogels after supercritical drying. Prior research suggests that the microstructure of silica aerogels aligns well with diffusion-limited aggregation-based (DLCA) models [14, 16].

Ma et al. [11, 17] further modified the DLCA model to describe the mechanical properties of silica aerogels, by treating bonds between particles as beams, since beams can capture the possible deformation of bonds including stretching, bending, and torsion. The study simulated hydrostatic compression on an off-lattice 2D DLCA model and obtained a power-law between bulk modulus $K$ and the volume fraction $\rho$ as $K \propto \rho^{3.6}$. Their subsequent study [18] showed that, with a linear elasticity formulation, the strain applied to the network does not affect the scaling exponent, implying the need to incorporate nonlinearity to study the strain–stress response. Recently, Abdusalamov et al. [12] extended this approach to 3D representative volume elements (RVEs) and subjected the RVEs to uniaxial compression using periodic boundary conditions (PBCs) in the finite element package. The mechanical characterizations of DLCA models have found that only a small portion of the bonds bear the majority of the load along certain backbone paths, leaving the rest stress-free. This phenomenon is also observed in colloidal materials [19].

More recently, Borzecka et al. [6] have developed a 3D diffusion-limited (DLCA) and reaction-limited (RLCA) aggregation model to study the kinetic curves. They obtained the relationship between porosity and collision probability, which is validated by both experimental and numerical results. Further investigations and studies on the applicability of the DLCA model for describing silica aerogels are referred to in recent reviews [19–21]. Armed with this knowledge, the present study seeks to explore more structural and mechanical details of DLCA models on silica aerogels.

This study will leverage the DLCA model to simulate the fractal structure of silica aerogels. The model assumes that the gel's structure remains unchanged during supercritical drying, thereby preserving the aerogel's structural integrity. This study will explore the mechanical behavior of aerogels under compression through simulations with the DLCA model, correlate the model's parameters to experimental findings, and examine how these parameters influence the properties of aerogels.

## 2 | METHODS

### 2.1 | Cluster–cluster aggregated model

In the context of gelation, structures composed of connected particles, referred to as "clusters" or "aggregates," eventually merge to form a single large cluster that spans the entire system. This single cluster transforms into a solid network in the solvent after the sol–gel process. To address the complexity of the cluster–cluster aggregation process, we employ DLCA models since Hasmy et al. [16] showed that these correlate best with the scattering data of silica aerogels. A unit cell in the shape of a cubic box has been chosen considering the cluster–cluster aggregates are not spherical [22].

The DLCA model developed by Abdusalamov et al. [12] is based on the diffusion-limited aggregation algorithm, in which a batch of particles is dropped into a given cubic volume with PBCs and undergoes random walks due to Brownian motion. In detail, the starting point is the initialization of particles, which are categorized into seeds and walkers. We denote the number of seeds and walkers as $N_S$ and $N_W$, respectively, so the number of particles will be $N_{all} = N_S + N_W$. Here, "seeds" are special particles that grow by incorporating "walkers" or merging with other "seeds." Thus, only particle–cluster and cluster–cluster bond formation occurs within the volume. The seeds are placed in an ordered fashion,
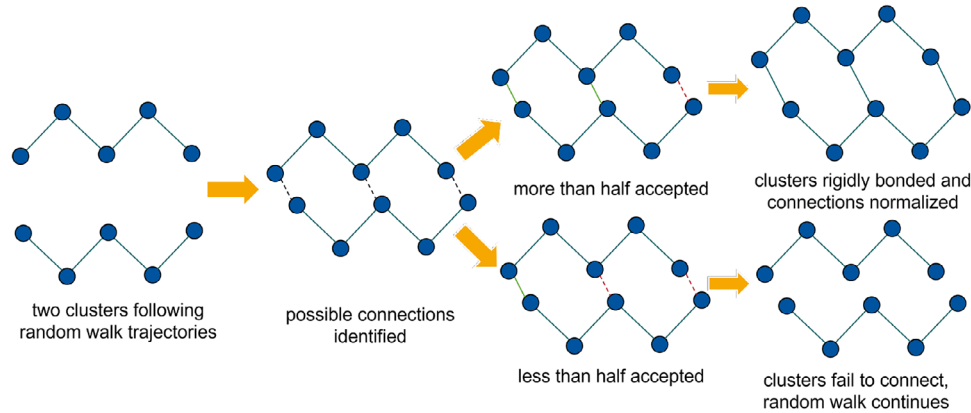
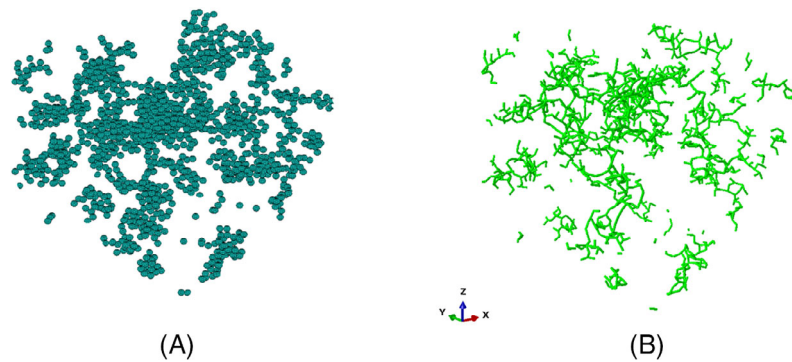**FIGURE 1** Sticking probability between clusters.



**FIGURE 2** (A) A DLCA model generated in a 200- nm cube with $\rho = 0.02$. (B) The FE-model transformed from the DLCA model.

while the walker particles are randomly initialized. The relative concentration, denoted as $\rho$, is the ratio of the particle volume $V_p$ to the bulk volume $V_b$

$$\rho = \frac{V_p}{V_b} = \frac{4\pi \sum_{i=1}^{N_{\text{all}}} r_i^3}{3L^3}, \tag{1}$$

with $r_i$ representing the individual particle radius and $L$ the size of the cubic box. As soon as a particle reaches a seed, its Brownian motion is stopped based on a critical distance $\epsilon_{\text{crit}}$ defined relative to seeds [12]. The particle diffuses and, with a sticking probability $p_s$, binds rigidly to the seed. The cluster–cluster aggregation [23] happens when several pairs of particles from two different clusters (seeds) reach their critical distance $\epsilon_{\text{crit}}$.

In contrast to the previous study [12], the sticking probability will be less than one ($0 < p_s < 1$); that is, the bond is not necessarily formed after reaching $\epsilon_{\text{crit}}$. The concept of sticking probability is similar to the acceptance ratio used in molecular dynamics trajectories [24, 25]. Borzęcka et al. [6] have recently demonstrated how the probability parameter, based on the Arrhenius equation, can show the relationship between synthesis parameters and model parameters, such as translating the time of gelation into the probability of an effective collision. The implementation of this study is as follows: the particle–cluster connection will be formed with a probability of $p_s$ upon reaching the $\epsilon_{\text{crit}}$, while the cluster–cluster connection is established only if more than 50% of potential connections between two clusters are formed (see also Figure 1).

## 2.2 | Finite element model

Strictly speaking, the models generated by DLCA (see Figure 2A) are purely mathematical construct at mesoscale without atomic degrees of freedom and the particles in models are rigid [1, 19, 26]. The methodological basis for determining the
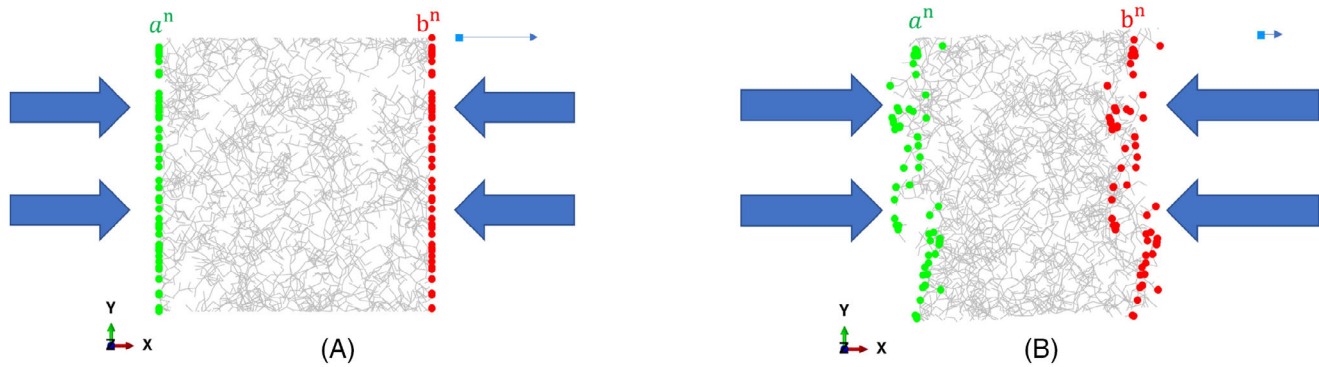
**FIGURE 3** View on X–Y-plane of the RVE (A) before compression (B) after compression caused by movement of dummy node.

mechanical properties involves transforming the DLCA model to a finite element model. We adopt the approach of Ma [17] for modeling bonds as beams, which is shown in Figure 2B. Specifically, the interparticle bonds were modeled using the B31 element type, a three-dimensional two-node Timoshenko beam element, in Abaqus.

To simulate the macroscopic response, PBCs have been applied to the model, treating the unit cell as a RVE. This model uses an implementation similar to that of Abdusalamov et al. [12]. This study applies a linear constraint to the boundary nodes using the "dummy node" concept as a method of implementing the PBC. The dummy node was introduced to indicate the bulk deformation of the cubic box. To maintain the integrity of the model, we constrained each pair of opposite boundary nodes, denoted as $a_i$ and $b_i$, using the following linear equation:

$$u_i^{a_j} - u_i^{b_j} = \delta_{ij} \hat{u}_i, \quad i, j \in \{1, 2, 3\}, \quad \left( x_i^{a_i} > x_i^{b_i} \right), \tag{2}$$

$$\psi_i^{a_j} = \psi_i^{b_j}, \quad i, j \in \{1, 2, 3\}, \tag{3}$$

where indexes $j$ indicates the direction of the boundary on which the nodes lie; $u_i$ and $\psi_i$ are the translational and rotational DOFs, respectively; $\delta_{ij}$ is the Kronecker delta whose value is 1 if the subscripts are equal ($i = j$) and 0 otherwise; $\hat{u}_i$ is the translational displacement of the dummy node. Figure 3A presents a view of the X–Y plane, showing a blue dummy node at the top corner of the box enforcing the PBC in the $x$-direction ($j = 1$) and constraining the dummy node with nodes from left and right boundaries, namely $u_i^{a_1} - u_i^{b_1} = \delta_{i1} \hat{u}_i$. The box will be compressed in the $x$-direction if the dummy nodes have positive displacement as shown in Figure 3B. After deformation, the boundary surfaces of the RVE do not remain flat; forcing flatness would over-constrain the RVE [27].

# 3 | RESULTS

In this study, DLCA models are generated in MATLAB. All models are generated within a cube of size $L = 200$ nm, as shown in Figure 2A, and have varying relative densities with a fixed seed number of $N_W = 9$. The particle radius $r = 3.1$ nm, the critical distance $\epsilon_{\text{crit}} = 2.3r$, and the particle step size $s = r/20$ are constants in the model.

A MATLAB script is also used to generate the input files for the finite element (FE) simulations of the DLCA models. The simulations are done in Abaqus 2020. The Young's modulus and Poisson's ratio of the beams are set to $E = 210000$ and $\nu = 0.3$, respectively. These values do not correspond to any physical material properties, as discussed in Ref. [11]. Large deformations of beam elements are considered. The results are discussed in this context.

## 3.1 | Structural characterization

To characterize the structural properties, the fractal dimension $d_f$ is evaluated as a function of relative density. This is determined by the relation between the mass $m(r)$ inside a sphere and the radius $r$ of the sphere. The sphere's placement
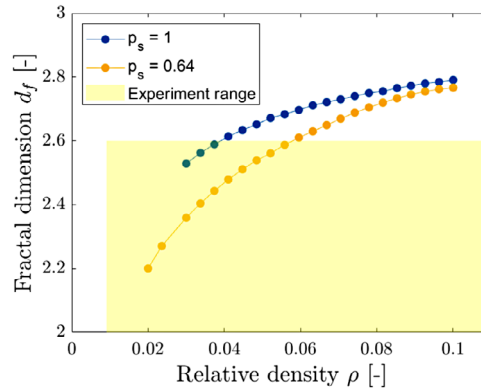
**FIGURE 4** Influence of the relative density and sticking probability on the fractal dimension.
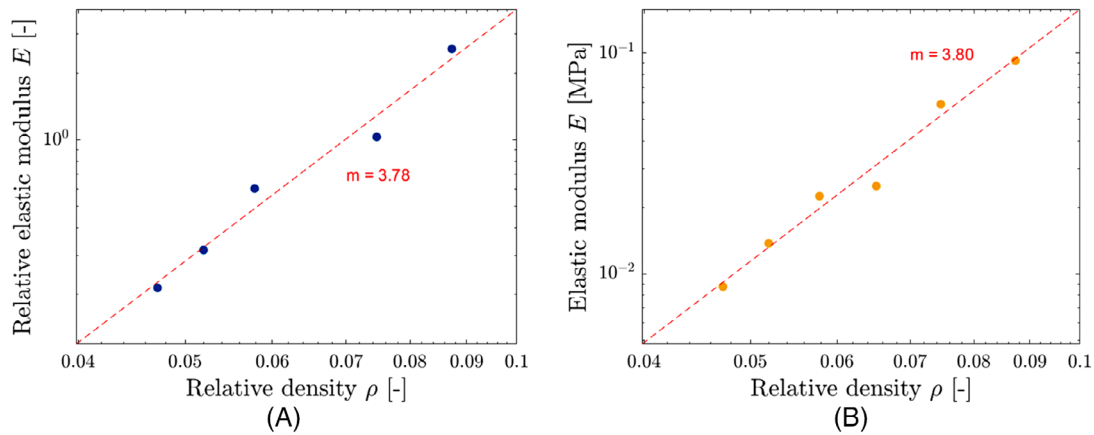


**FIGURE 5** (A) Log-log plot of the elastic modulus versus the relative density from simulation. (B) Plot of experimental data.

can be arbitrary due to the assumed periodicity of the unit cell. At the nanometer length scale, the relationship can be precisely described by $m(r) \propto r^{d_f}$, where $d_f$ is the slope of the function when plotted in a log–log scale. The obtained fractal dimensions are collected and plotted as a function of $\rho$ in Figure 4, which also includes the influence of the probability $p_s$. For $p_s = 1$, the curve is exactly the same as in the previous study [12]. As the probability decreases, so does the fractal dimension, resulting in a highly porous structure. The common range of fractal dimension reported by recent experiments [5, 19, 21] is highlighted in yellow in Figure 4. As the density increases beyond 0.1, the fractal dimension tends to approach close packing with $d_f = 3$. Hsieh et al. [13] reported a similar phenomenon for the 3D DLCA model at a relative density greater than 0.05, concluding that the Langevin dynamics approach is more realistic for a constant size of the unit cell. However, since the fractal dimension decreases with decreasing probability $p_s$, the DLCA model should also be able to reproduce the fractal dimensions observed in aerogels with higher densities.

## 3.2 | Mechanical characterization

As described in Section 2.2, we export the DLCA models discussed above to the Abaqus/CAE software package to subject them to compression tests.

The focus is first on the elastic model. By averaging the FE models' responses, we obtain isotropic mechanical behavior, allowing for the determination of Young's modulus in the linear elastic region (at $\epsilon \approx 0.01$). The relationship between Young's modulus and density can be described as a power law $E \propto \rho^m$ with a scaling exponent $m$. In our simulations, as shown in Figure 5A, the value of $m$ is found to be 3.78, which correlates well with the experimentally obtained value of $m = 3.80$. Additionally, the Poisson's ratio $\nu$ of the unit cell can be determined, since it is subjected to uniaxial compression. The Poisson's ratio $\nu$, as shown in Figure 6A, is generally insensitive to the densities, which agrees with Ma's findings [17].
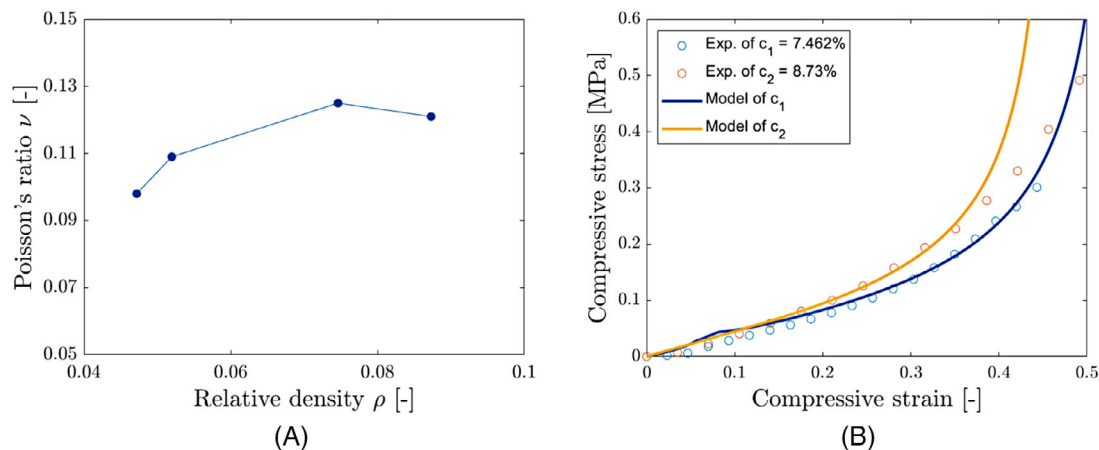
**FIGURE 6** (A) Poisson's ratio obtained from simulation. (B) Comparison of stress–strain response of the model with the experimental results.

This insensitivity suggests a power law relationship between bulk modulus $K$ and density $\rho$, characterized by the same exponent $m$ ($K \propto \rho^m$). However, the response correlates well with the experiment only in the linear elastic region up to 3%. To accurately describe the nonlinear response beyond this point, additional nonlinear factors should be included.

Inclusion of contact interaction means inclusion of nonlinear boundary conditions. For dense aerogels, the model shows a quantitatively good agreement with experimental data up to 40% compressive strain as shown in Figure 6B. Furthermore, we observed that the model can successfully capture the three stages of the compression test, namely the linear, plateau, and densification stages. To correlate at larger compressive strains ($\epsilon > 0.4$), an elasto-plastic model is needed to capture yielding and a failure model is needed to predict where damage will occur.

## 4 | SUMMARY

In this study, we developed a coarse-grained model for silica aerogels based on diffusion-limited cluster–cluster aggregation (DLCA) with additional consideration of sticking probability. This approach allowed us to replicate the classical structure of silica aerogels for a wider range of relative densities, effectively capturing their key features while reducing complexity and simulation time. Our finite element model was able to reproduce the compressive response of these unique materials. Furthermore, the model's response at low compressive strains is in good agreement with experimental data, demonstrating its capability. By incorporating elastic, plastic, and failure models, we expect to gradually gain valuable insights into the behavior of aerogels under compressive loading conditions. While our model has provided correlated results, further refinements are needed to develop a more applicable model for the mechanical behavior of silica aerogels. More physics-based implementations, such as the diffusion coefficient satisfying the Einstein–Stokes equation and varying particle neck size, could be incorporated for better understanding in material properties and reverse engineering.

**ORCID**
*Weibo Xiong* https://orcid.org/0009-0000-8332-0787
*Rasul Abdusalamov* https://orcid.org/0000-0003-4988-4794
*Ameya Rege* https://orcid.org/0000-0001-9564-5482

**REFERENCES**
1. Gelb, L. D. (2023). *Simulation and modeling of aerogels using atomistic and mesoscale methods.* In M. A. Aegerter, N. Leventis, M. Koebel, & S. A. Steiner III (Eds.), Springer handbook of aerogels (pp. 273–288). Springer International Publishing.
2. Steiner, S. A., & Pierre, A. C. (2023). *The story of aerogel.* In M. A. Aegerter, N. Leventis, M. Koebel, & S. A. Steiner III (Eds.), Springer handbook of aerogels (pp. 1–50). Springer International Publishing.

3. Luo, H., Malakooti, S., Churu, H. G., Leventis, N., & Lu, H. (2023). *Mechanical characterization of aerogels*. In M. A. Aegerter, N. Leventis, M. Koebel, & S. A. Steiner III (Eds.), Springer handbook of aerogels. (pp. 197–229). Springer International Publishing.

4. Anderson, A. M., & Carroll, M. K., (2023). *Hydrophobic silica aerogels*. In M. A. Aegerter, N. Leventis, M. Koebel, & S. A. Steiner III (Eds.), Springer handbook of aerogels (pp. 335–365). Springer International Publishing.

5. Gonçalves, W., Morthomas, J., Chantrenne, P., Perez, M., Foray, G., & Martin, C. L. (2018). Elasticity and strength of silica aerogels: A molecular dynamics study on large volumes. *Acta Materialia*, *145*, 165–174.

6. Borzęcka, N. H., Nowak, B., Pakuła, R., Przewodzki, R., & Gac, J. M. (2023). Diffusion/reaction limited aggregation approach for microstructure evolution and condensation kinetics during synthesis of silica-based alcogels. *International Journal of Molecular Sciences*, *24*(3), 1999.

7. Barbero, E., & Campo, F. (2012). Sol-gel simulation-II: Mechanical response. *Journal of Non-Crystalline Solids*, *358*(4), 728–734.

8. Ratke, L., & Hajduk, A. (2015). On the size effect of gelation kinetics in RF aerogels. *Gels*, *1*(2), 276–290.

9. Gelb, L. D. (2007). Simulating silica aerogels with a coarse-grained flexible model and Langevin dynamics. *The Journal of Physical Chemistry C*, *111*(43), 15792–15802.

10. Ferreiro-Rangel, C. A., & Gelb, L. D. (2013). Investigation of the bulk modulus of silica aerogel using molecular dynamics simulations of a coarse-grained model. *The Journal of Physical Chemistry B*, *117*(23), 7095–7105.

11. Ma, H. S., Roberts, A. P., Prévost, J. H., Jullien, R., & Scherer, G. W. (2000). Mechanical structure–property relationship of aerogels. *Journal of Non-Crystalline Solids*, *277*(2-3), 127–141.

12. Abdusalamov, R., Scherdel, C., Itskov, M., Milow, B., Reichenauer, G., & Rege, A. (2021). Modeling and simulation of the aggregation and the structural and mechanical properties of silica aerogels. *The Journal of Physical Chemistry B*, *125*(7), 1944–1950.

13. Hsieh, K., Lallet, F., & Olivi-Tran, N. (2008). DLCA and Langevin dynamics approaches of sol gel transition: A comparison via the fractal dimension during aggregation. *Fractals*, *16*(04), 361–365.

14. Hasmy, A., Foret, M., Pelous, J., & Jullien, R. (1993). Small-angle neutron-scattering investigation of short-range correlations in fractal aerogels: Simulations and experiments. *Physical Review B*, *48*, 9345–9353.

15. Hasmy, A., Foret, M., Anglaret, E., Pelous, J., Vacher, R., & Jullien, R. (1995). Small-angle neutron scattering of aerogels: Simulations and experiments. *Journal of Non-Crystalline Solids*, *186*, 118–130.

16. Hasmy, A., Anglaret, E., Foret, M., Pelous, J., & Jullien, R. (1994). Small-angle neutron-scattering investigation of long-range correlations in silica aerogels: Simulations and experiments. *Physical Review B*, *50*, 6006–6016.

17. Ma, H. S., Prévost, J. H., Jullien, R., & Scherer, G. W. (2001). Computer simulation of mechanical structure–property relationship of aerogels. *Journal of Non-Crystalline Solids*, *285*(1-3), 216–221.

18. Ma, H. S., Prévost, J. H., & Scherer, G. W. (2002). Elasticity of DLCA model gels with loops. *International Journal of Solids and Structures*, *39*(18), 4605–4614.

19. Rege, A. (2023). *Modeling the structural, fractal and mechanical properties of aerogels*. In M. A. Aegerter, N. Leventis, M. Koebel, & S. A. Steiner III (Eds.), Springer handbook of aerogels (pp. 289–305). Springer International Publishing.

20. Patil, S. P., Parale, V. G., Park, H. H., & Markert, B. (2021). Mechanical modeling and simulation of aerogels: A review. *Ceramics International*, *47*(3), 2981–2998.

21. Woignier, T., Primera, J., Alaoui, A., Dieudonne, P., Duffours, L., Beurroies, I., Calas-Etienne, S., Despestis, F., Faivre, A., & Etienne, P. (2021). Fractal structure in silica and composites aerogels. *Gels*, *7*(1), 1.

22. Meakin, P. (1999). A historical introduction to computer models for fractal aggregates. *Journal of Sol-Gel Science and Technology*, *15*(2), 97–117.

23. Meakin, P. (1984). Diffusion-limited aggregation in three dimensions: Results from a new cluster-cluster aggregation model. *Journal of Colloid and Interface Science*, *102*(2), 491–504.

24. Clamp, M. E., Baker, P. G., Stirling, C. J., & Brass, A. (1994). Hybrid monte carlo: An efficient algorithm for condensed matter simulation. *Journal of Computational Chemistry*, *15*(8), 838–846.

25. Beskos, A., Pillai, N. S., Roberts, G. O., Sanz-Serna, J. M., & Stuart, A. M. (2010). The Acceptance Probability of the Hybrid Monte Carlo Method in High-Dimensional Problems. *AIP Conference Proceedings*, *1281*(1), 23–26.

26. Liu, Q., Lu, Z., Zhu, M., Yuan, Z., Yang, Z., Hu, Z., & Li, J. (2014). Simulation of the tensile properties of silica aerogels: The effects of cluster structure and primary particle size. *Soft Matter*, *10*, 6266–6277.

27. Omairey, S. L., Dunning, P. D., & Sriramula, S. (2019). Development of an Abaqus plugin tool for periodic RVE homogenisation. *Engineering with Computers*, *35*(2), 567–577.